Atmos. Chem. Phys., 10, 8119–8130, 2010
www.atmos-chem-phys.net/10/8119/2010/
doi:10.5194/acp-10-8119-2010

Atmospheric Chemistry and Physics

Haze types in Beijing and the influence of agricultural biomass burning

W. J. Li[1,2,3], **L. Y. Shao**[2], **and P. R. Buseck**[3]

[1]Environment Research Institute, Shandong University, Jinan, Shandong 250100, China
[2]State Key Laboratory of Coal Resources and Safe Mining & College of Geoscience and Surveying Engineering, China University of Mining and Technology, Beijing 100083, China
[3]School of Earth and Space Exploration & Department of Chemistry and Biochemistry, Arizona State University, Tempe, AZ 85287-1404, USA

Received: 26 January 2010 – Published in Atmos. Chem. Phys. Discuss.: 22 April 2010
Revised: 17 August 2010 – Accepted: 26 August 2010 – Published: 1 September 2010

Abstract. Emissions from agricultural biomass burning (ABB) in northern China have a significant impact on the regional and global climate. The monthly average aerosol optical depth (AOD) at 550 nm in northern China in 2007 had a maximum of 0.7 in June. The AOD measurements are consistent with regional brown hazes that occurred at that time, which was a period of severe aerosol pollution. Aerosol particles were collected in urban Beijing from 12 to 30 June 2007, during a period of high haze, and studied using transmission electron microscopy with energy-dispersive X-ray spectrometry. The dominant particle types collected in the fine fraction (diameter <1 μm) were ammonium sulfate, soot, K_2SO_4, KNO_3, and organic matter, except that the K salts were minor between 21 and 30 June. K-rich particles as tracers of biomass burning, together with wildfire maps, show that intense regional ABB in northern China contributed significantly to the regional haze between 12 and 20 June. We therefore grouped the episodes into type-1 and -2 haze, with the former occurring between 12 and 20 June and the latter between 21 and 30 June. After long-range transport, ABB particles in the type-1 haze exhibited marked changes in morphology, composition, and mixing state. KCl particles were absent, presumably having been converted by heterogeneous reactions to K_2SO_4 and KNO_3. Soot particles were mixed with the other particle types. Abundant organic matter and soluble salts emitted by ABB increased their sizes during transport and resulted in more hygroscopic aerosol particles in downwind areas, becoming additional cloud condensation nuclei. The high AOD (average value 2.2) in Beijing during 12 to 20 June is partly explained by the hygroscopic growth of fine aerosol particles and by the strong absorption of internally mixed soot particles, both coming from regional ABB emissions. Therefore, it is important to consider the origins of the haze, which in turn leads to the different particle types.

Correspondence to: L. Y. Shao
(shaol@cumtb.edu.cn)

1 Introduction

Biomass burning is a global phenomenon that releases large quantities of gases and aerosol particles that affect the atmospheric chemistry and climate by scattering and absorbing solar radiation on regional and global scales (Crutzen and Andreae, 1990). Aerosol particles from biomass burning also dramatically increase the concentration of cloud condensation nuclei (CCN) and affect the formation and lifetime of clouds (Andreae et al., 2004; Roberts et al., 2003). Such aerosol particles serving as CCN also alter the radiation budget of clouds in the troposphere (IPCC, 2007). In addition, because of the transport of biomass-burning particles with nutrient species (e.g., S, K, and N) from agricultural regions into urban areas, these aerosols alter the regional biogeochemical cycling and adversely affect human health (Bowman et al., 2009; Crutzen and Andreae, 1990; Da Rocha et al., 2005; Koe et al., 2001; Niemi et al., 2005; Reid et al., 2005).

Agricultural biomass burning (ABB) in China is drawing worldwide attention because of its rapid development and increase in agricultural activities. Numerous studies have shown that the mixtures of pollutants from industries, biomass burning, and urban areas in northern China can be transported over the Pacific Ocean (Jacob et al., 2003; Ma et al., 2003) into North America and thus cause problems across

wide areas (de Gouw et al., 2004; Jaffe et al., 1999; Peltier et al., 2008; Yienger et al., 2000).

Compared with plumes from soil dust and industrial emissions, as well as with relatively clean air masses, those over northern China that contain emissions from ABB show distinct optical properties (Yang et al., 2009). In particular, massive quantities of fine soot particles (also known as black carbon or elemental carbon) are emitted into the troposphere. According to Ramanathan and Carmichael (2008), soot in the troposphere is the second greatest contributor to global warming after CO_2.

In the atmosphere, soot particles commonly acquire coatings of sulfates, organic matter, and sulfuric acid (Adachi and Buseck, 2008; Adachi et al., 2010; Johnson et al., 2005; Pósfai et al., 1999), thereby enhancing the light absorption of soot (Chung and Seinfeld, 2002; Jacobson, 2001; Lesins et al., 2002; Zhang et al., 2008). For example, particles coated with sulfate absorb 30% more light than soot alone (Fuller et al., 1999). Clearly, a complete physical and chemical investigation of ambient ABB aerosol particles, most particularly soot particles, must be conducted before the climate impacts of aerosols can be evaluated for China.

In recent studies of ABB from China, Cao et al. (2008) estimated that emissions from straw burning amount to 140 Tg/year. Duan et al. (2004) found that monthly average concentrations of K in Beijing were three times higher in June than in May, likely because of ABB emissions. Zhang et al. (2007) showed that such emissions increased both organic and elemental carbon concentrations and that smoldering and flaming significantly influenced the formation of elemental carbon and polycyclic aromatic hydrocarbons (PAHs).

In spite of the above studies, information is lacking about the composition and mixing states of aged ABB aerosol particles in urban regions and their impacts on regional climate. Two reasons explain this situation. First, ABB emissions occur at different times within the spring season because timing of farming activities change with latitude throughout China. Therefore, flexible sampling schedules are needed. Second, the frequent episodes of severe pollution with high mass concentrations of particulate matter (PM) from industrial and vehicular emission in urban areas may mask ABB aerosols, suggesting that bulk analytical methods cannot adequately identify such particles. Also, bulk methods, which focus on the composition of aerosol particle obtained from relatively long sampling periods, are unable to identify ABB particles during those episodes. In addition, bulk methods only provide information about aerosol mixtures, not individual ABB particles.

In contrast, individual-particle analysis using transmission electron microscopy (TEM) provides detailed information on individual particles at a high resolution (Buseck and Pósfai, 1999; Pósfai and Buseck, 2010; Johnson et al., 2005). TEM is uniquely suited for observing and analyzing the morphology, size, structure, and mixing state of such aerosol particles (Johnson et al., 2005; Pósfai et al., 1999; Li and Shao, 2009b).

The goal of this paper is to determine the properties of individual ABB particles that are significant contributors to the regional brown hazes in northern China and that are prominent in Beijing. K-rich aerosol particles serve as tracers of biomass burning and, together with wildfire maps, were used to identify regional ABB sources for the hazes. Using TEM, particular attention was paid to the phase and mixing state of individual aerosol particles. Air-mass backtrajectories, satellite observations of fires, and aerosol optical depth (AOD) measurements from sun photometers were used to evaluate the effects of ABB-related aerosol particles in the brown hazes.

2 Materials and methods

2.1 Aerosol sampling and laboratory preparations

Aerosol particles were collected during seven haze episodes between 12 and 27 June 2007 in northwestern urban Beijing (39°59° N, 116°20° E) (Table 1). Samplers were mounted 18 m above ground on the roof of a building on the campus of the China University of Mining and Technology. Particles were collected onto copper TEM grids coated with carbon film (carbon type-B, 300-mesh copper, Tianld Co., China) using a single-stage cascade impactor with a 0.5-mm-diameter jet nozzle with a flow rate of $1.0\,\mathrm{L\,min^{-1}}$. Sampling times varied from 30 to 120 s, depending on the visibility and thus likely particle loading. Measurements of wind speed, wind direction, relative humidity, barometric pressure, and ambient temperature were automatically recorded by a Kestral 4000 Pocket Weather Tracker (Nielsen-Kellermann Inc., USA) (Table 1). After collection, each sample was placed in a sealed dry plastic tube and stored in a desiccator at 25 °C and 20±3% RH to minimize exposure to ambient air and preserve it for analysis.

Additionally, K_2SO_4 and KNO_3 aerosol particles were generated from $1M$ solutions prepared from analytical reagent-grade chemicals (97% purity, Aldrich). The particles were dried using a silicon diffusion drier (TSI Model 3062) to an RH of 20% (TSI, 2003). Single particles were deposited by diffusion onto TEM grids, a technique described by Freney et al. (2009).

2.2 TEM analysis

Aerosol particles were analyzed with a Philips CM200 TEM operated at 200 kV. The distribution of aerosol particles on the TEM grids was not uniform. Coarser particles were deposited near the center of the grids and finer particles on the periphery. Therefore, to ensure that the analyzed particles were representative of the entire size range, three to four areas were chosen from the center and periphery of the sampling spot on each grid. An ellipse was used to fit a particle

Table 1. Information on analyzed samples from urban Beijing.

Date	Start Time	T	RH[a]		P	WS	WD	V
	UTC	°C	mean, %	max, %	hPa	($m\,s^{-1}$)		km
12/06/2007	09:30	20	62	67	1000	2	SE	3
17/06/2007	09:45	30	42	48	999	3	SSE	4
19/06/2007	02:30	31	44	51	1004	2	WSS	3
19/06/2007	05:30	32	50	53	1002	1	SSE	0.5
20/06/2007	07:00	28	66	69	1001	3	S	2
21/06/2007	03:00	36	36	39	999	2	WS	3
23/06/2007	04:00	28	62	65	993	2	SE	3
23/06/2007	04:10	28	62	65	993	2	SE	3
27/06/2007	02:00	32	64	67	991	3	SEE	2
27/06/2007	02:10	32	64	67	991	3	SEE	2
27/06/2007	05:45	24	70	75	991	8	WSS	4

T – temperature, RH – relative humidity, P – barometric pressure, WS – wind speed, WD – wind direction, V – visibility.
[a] RH includes mean and maximum value during each sampling period.

outline, and the arithmetic mean of the short and long axes of the ellipse was used to determine the particle diameter (Pósfai et al., 2003).

Elemental compositions were determined semi-quantitatively by using an energy-dispersive X-ray spectrometer (EDS) that can detect elements heavier than C. For some particles, EDS data were combined with selected-area electron diffraction (SAED) to verify their identities. Copper was not considered because of interferences from the copper TEM grid. To understand the details of internally mixed aerosol particles and their sources, the compositions of different parts of targeted aerosol particles were analyzed (e.g., coatings, inclusions, and aggregations). EDS spectra were collected for 30 s in order to minimize radiation exposure and potential beam damage. Prior TEM observations of the major aerosol types collected in brown hazes from 30 May to 10 June 2007 revealed mineral, soot, organic matter, K-rich, S-rich, fly ash, and metal particles (Li and Shao, 2009a). In the current study, we focused on the soot, organic matter, K-rich, and S-rich particles.

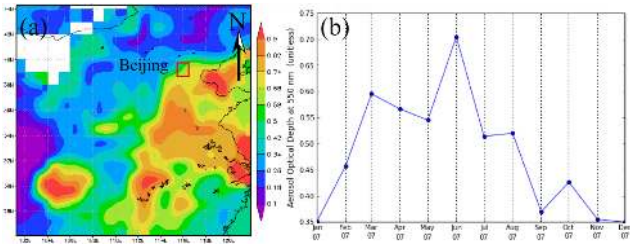

Fig. 1. Aerosol optical depth (AOD) map and monthly average AOD of area-averaged time series over northern China (region: 101.25 E–121.99 E, 26.02 N–44.30 N) derived from MODIS-Terra data from January to December 2007 (http://disc.sci.gsfc.nasa.gov/giovanni/). **(a)** Mean AOD value at 550 nm from January to December 2007. **(b)** Monthly mean AOD value in 2007.

3 Results

3.1 Regional haze in northern China

The regional distribution of aerosols and AOD were obtained from Giovanni maps [Giovanni is an acronym for the *G*ES-DISC (Goddard Earth Sciences Data and Information Services Center) *I*nteractive *O*nline *V*isualization *AN*d a*N*alysis *I*nfrastructure] from MODIS (Moderate Resolution Imaging Spectroradiometer) satellite data (Acker and Leptoukh, 2007). These data indicate that severe aerosol pollution occurred in northern China (Fig. 1a), with a maximum monthly average AOD at 550 nm of 0.7 in June 2007 (Fig. 1b). Such a high value indicates high PM loading in the troposphere and is related to severe pollution episodes such as regional brown hazes or dust storms (Du et al., 2008; Eck et al., 1999).

Asian dust storms usually begin in late February and end in mid-May (Shao et al., 2008; Zhang et al., 2003). Therefore, the regional pollution episodes in June are more likely to be the brown hazes, consistent with our observations at the sampling site. The aerosols in the regional hazes were largely contributed by anthropogenic sources such as industrial emissions, vehicular fossil fuel combustion, and ABB (Li and Shao, 2009a). The hazy days had visibility less than 5 km, wind speeds less than $3\,m\,s^{-1}$, and winds from south of Beijing (Table 1). The regional hazes disappeared in half a day or less because of the onset of abrupt cold fronts from the west, and then formed again within a day or less during the sampling period. The daily mass concentrations of PM_{10} and SO_2 in June displayed dramatic changes (Fig. 2), consistent with the visual observations of the haze. The

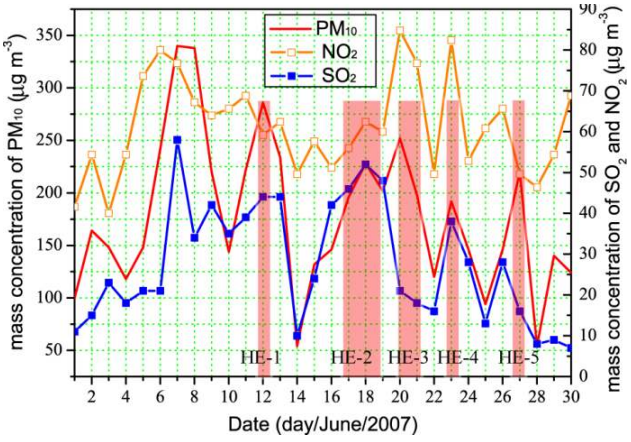

Fig. 2. Daily mass concentrations of PM_{10}, SO_2, and NO_2 in Beijing in June 2007 (http://datacenter.mep.gov.cn/). Sample collection was conducted during the five haze episodes (HE-1, HE-2, HE-3, HE-4, and HE-5) indicated by the orange vertical bars. Widths of the bars indicate the haze periods.

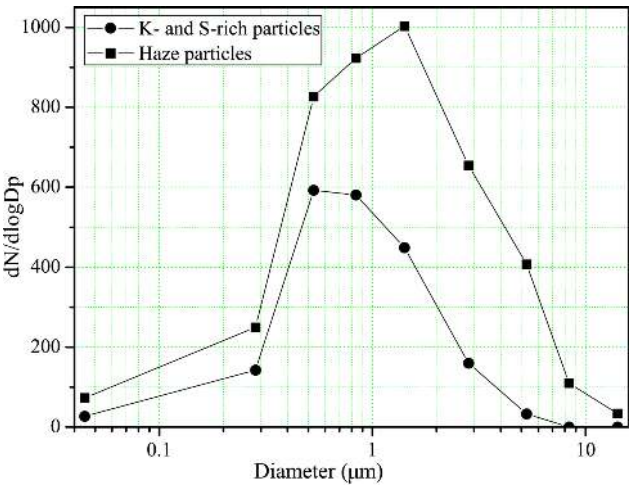

Fig. 3. Size distributions of 1066 haze particles (i.e., mineral, soot, organic matter, K-rich, S-rich, fly ash, and metal particles) and 470 K- and S-rich particles. The size distributions represent the fraction sampled rather than the total collection of aerosol particles. Most K- and S-rich particles were internally mixed with soot, organic matter, or both.

frequent alternation between clear and hazy days is conspicuously noticeable in what Jia et al. (2008) called a sawtooth cycle. Eleven samples collected in the five haze episodes (HE-1, HE-2, HE-3, HE-4, and HE-5) were selected for detailed analysis (Fig. 2).

Mass concentrations of PM_{10}, SO_2, and NO_2 on hazy days ranged from 192 to 286 $\mu g\,m^{-3}$, 16 to 48 $\mu g\,m^{-3}$, and 50 to 83 $\mu g\,m^{-3}$, respectively (data provided by the Beijing Meteorological Bureau). Pollutants on hazy days (peaks in the sawtooth cycle) showed mass concentrations 2 to 3 times higher than pollutants on clear days (valleys in the sawtooth cycle), suggesting that the stable meteorological conditions on hazy days favored the accumulation of air pollutants that were then slowly transported into adjacent areas.

3.2 Major fine aerosol particles and their size distributions

In this section, we describe the different kinds of particles in the brown hazes. We then combine these results with the MODIS data to identify those specifically related to ABB in section 3.3. The experimental data are based on TEM analysis of individual aerosol particles from the brown haze episodes. We distinguished seven kinds of aerosol particles: mineral, soot, organic matter, fly ash, and K-rich, S-rich, and metal particles (Li and Shao, 2009a). Sizes of the 1066 analyzed haze particles collected between 12 and 27 June range from 0.01 to 13 μm, with a median diameter of 1.4 μm (Fig. 3). Sizes of the 470 K- and S-rich particles range from 0.01 to 10 μm, with a median diameter of 0.7 μm.

K-rich particles, one of the abundant inorganic aerosol constituents of the brown hazes, are regarded as tracers of biomass burning and biofuel emissions (Reid et al., 2005; Adachi and Buseck, 2008; Engling et al., 2009). Most K-rich particles are irregularly shaped. EDS measurements show that they consist mostly of N, Na, O, S, and K and are free of Cl (Fig. 4). Diffraction patterns indicate the presence of K_2SO_4 and KNO_3, and they are internally mixed (Fig. 4). The KNO_3 is more beam-sensitive than the K_2SO_4, making good diffraction patterns of KNO_3 difficult to obtain. These EDS and SAED results are consistent with our observations of laboratory-generated K_2SO_4 and KNO_3 particles. KCl is barely detected in the samples, even though it has been found to be internally mixed with K_2SO_4 and KNO_3 in fresh biomass burning plumes (Li et al., 2003; Adachi and Buseck, 2008).

S-rich particles, another of the abundant inorganic aerosol constituents of brown hazes, appear as subrounded masses on TEM grids, with their principal elements being N, O, S, and minor Na and K (Fig. 5). Their SAED patterns indicate most are ammonium sulfate ($(NH_4)_2SO_4$). In addition, sulfate particles with one or more rings of smaller particles (Fig. 5) suggest that they are somewhat more acidic than pure ammonium sulfate (Buseck and Pósfai, 1999; Sheridan et al., 1993). The abundant $(NH_4)_2SO_4$ particles in Beijing air have been reported to form through chemical reactions between NH_3 and H_2SO_4 (Yao et al., 2003).

Soot particles are abundant in urban air and commonly occur as inclusions in or associated with K- and S-rich particles (Johnson et al., 2005; Adachi and Buseck, 2008; Li and Shao, 2009a; Adachi et al. 2010). The soot particles display their characteristic morphologies of chains and agglomerates (Fig. 6a). High-magnification TEM images show that some aggregates contain as few as ten to as many as hundreds of carbon spheres, with diameters from 10 to 50 nm and with

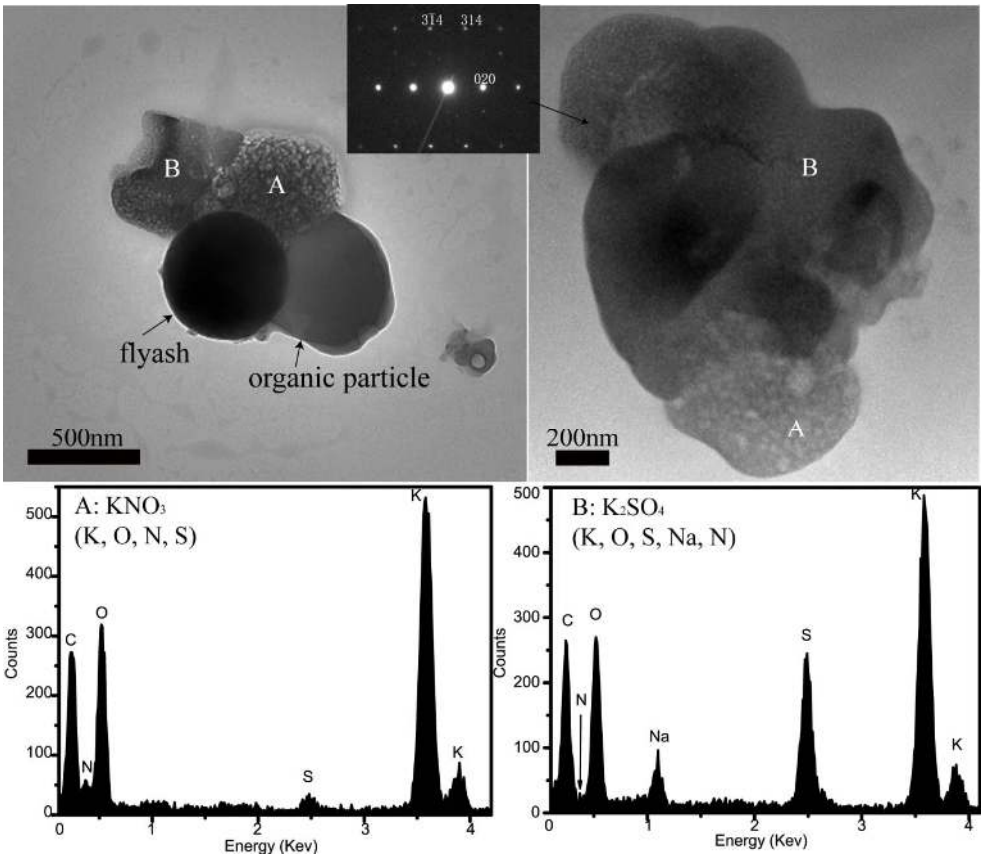

Fig. 4. Mixtures of **(a)** KNO_3 and **(b)** K_2SO_4 from samples collected on 17 June (left) and 19 June (right), respectively, based on their compositions and crystal structures from EDS and SAED measurements. The inset shows an indexed diffraction pattern of K_2SO_4. KNO_3 is more beam-sensitive than K_2SO_4.

some as large as 100 nm. As is typical, the soot spheres display the onion-like structures of disordered graphitic layers (Fig. 6b).

Although volatile and some semi-volatile chemical species evaporate in the high vacuum of electron microscopes, individual-particle analysis using electron microscopy has been used to study non-volatile particles, including organic matter and its mixing characteristics in the atmosphere (Pósfai et al., 2003; Niemi et al., 2005; Adachi and Buseck, 2008; Li and Shao, 2010). Much of the organic matter contains C and minor N, O, S, and K and lacks graphitic, soot-like structures in high-resolution TEM images (Fig. 6). It typically displays rounded, relatively non-descript shapes and commonly coats or embeds other particle types such as the K-rich, S-rich, and soot particles.

3.3 Identification of the regional hazes affected by agricultural biomass burning

ABB and its associated impacts on Beijing air were reported by Li et al. (2008) and Duan et al. (2004), who showed that the intense ABB in some provinces (e.g., Shandong, Hebei, Henan, Anhui) of northern China is usually concentrated in June. MODIS wildfire maps show that intense ABB occurred in northern China between 10 and 20 June 2007,and that slight ABB occurred between 21 and 30 June (Fig. 7).

Many K-rich particles and some S-rich particles occurred during the former period, whereas the opposite situation existed during the second period. The abundance of K-rich particles in the haze between 12 and 20 June probably arose from biomass burning, consistent with the results of Reid et al. (1998), Pósfai et al. (2003), and Engling et al. (2009). Samples were collected during that period, and air masses during the HE-1, HE-2, and HE-3 episodes were transported through the area with intense ABB. Air masses during HE-4 and HE-5 were transported through areas with slight ABB (Fig. 7). Prevailing southerly or southeasterly winds (Table 1) likely carried large amounts of fine ABB particles over long distances into the regional haze of Beijing during the period 12 to 20 June.

Using wildfire maps and individual-particle analysis, we distinguished between what we call type-1 and -2 haze, with the former occurring between 12 and 20 June and the latter between 21 and 30 June. Figure 8a, which is based on 470

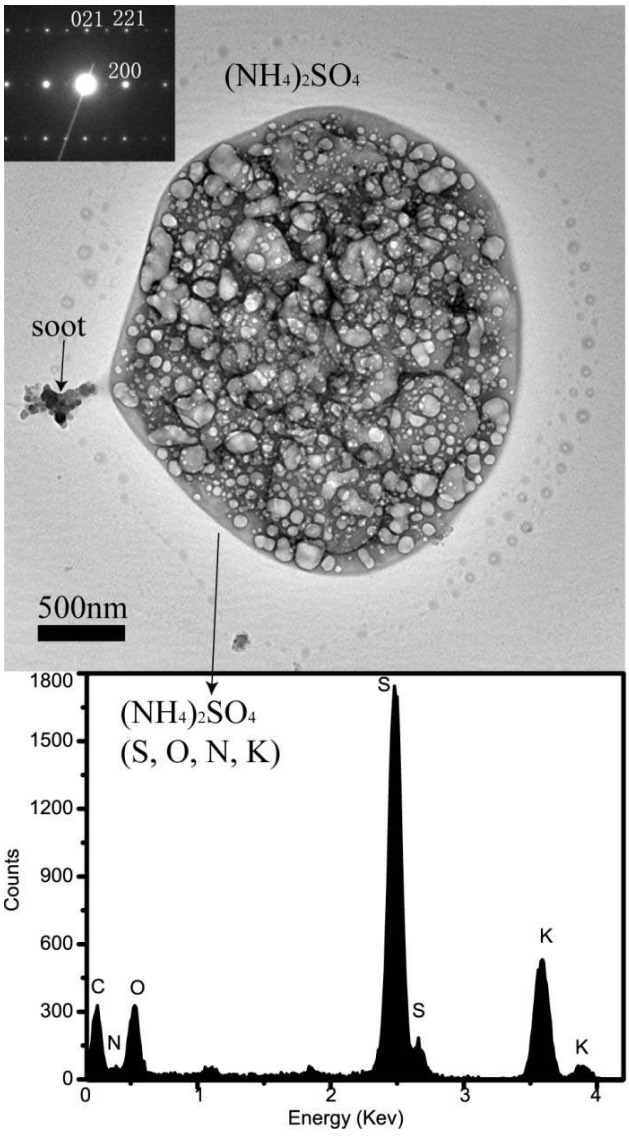

Fig. 5. TEM image and element content (S, N, O, and K) of S-rich particle (23 June). The diffraction pattern was obtained from a similar-looking particle, which was destroyed during electron-beam exposure.

K- and S-rich particles, shows that 65% of aerosol particles in type-1 haze fall to the left of the K_2SO_4 line, while only 9% in type-2 haze do. The particles to the left of the K_2SO_4 line are enriched in K and contain minor S. Based on the EDS measurements and SAED analysis, the major particles on the left are dominated by K_2SO_4, KNO_3, or mixtures of both (Figs. 4 and 7b). The low-magnification TEM images also show that there are more complex mixtures of the K-rich and S-rich particles (Fig. 8b) from type-1 haze than the S-rich particles (Fig. 8c) from type-2 haze. On the other hand, mean values of AOD and water vapor content (WVC) between 12 and 20 June were 2.0 and 2.2, respectively (Fig. 9). The mean values of AOD and WVC during the period 21 to 28 June were 1.1 and 2.7, respectively (Fig. 9).

4 Discussion

4.1 Effects of ABB emissions on the brown hazes

Transported ABB emissions not only increased the atmospheric loading but also changed the chemical and physical properties of aerosol particles in downwind areas. Brown hazes over northern China are normally produced by emissions from industry, fossil fuels (e.g., vehicles and cooking), and soil dust from natural and anthropogenic activities (Li and Shao, 2009a). We assumed that these sources had a constant emission rate throughout the period of the study. During the sampling period, daily average mass concentrations of PM_{10} and SO_2 between 12 and 20 June and 21 and 30 June decreased from 192 $\mu g\,m^{-3}$ to 143 $\mu g\,m^{-3}$, and from 37 $\mu g\,m^{-3}$ to 18 $\mu g\,m^{-3}$, respectively (Fig. 2). We infer from wildfire maps (Fig. 7) that the intense ABB emissions in type-1 haze increased the loading of PM_{10} and SO_2 in Beijing air.

ABB can emit large quantities of fine primary particles (e.g., organic matter and K-rich particles), soot, and gases (e.g., VOCs, CO, NO_x, SO_2, and NH_3) into the troposphere (Crutzen and Andreae, 1990). Reid et al. (1998) estimated that condensation and gas-to-particle conversions of vapors from biomass burning increased the aerosol mass by 20 to 40%. In addition, the mean WVC value is slightly higher in type-2 haze than in type-1 haze (Fig. 9), consistent with the RH measurements in Fig. S1. However, type-1 haze has a mean AOD double that of the type-2 haze in this study (Fig. 9). The most logical explanation is that the intense ABB emissions in the type-1 haze increased the AOD.

Internally mixed fine particles are common in the hazes (Fig. 8b). Soot and organic matter occur as inclusions in K- and S-rich particles (Fig. 10), and only small quantities of externally mixed organic matter and soot particles were observed on the TEM grids that sampled the hazes. The result is consistent with our investigation of aerosol particles in the brown hazes from 31 May to 11 June (Li and Shao, 2009a). The soot particles in Fig. 10e–g became hydrophilic when they were coated with water-soluble compounds such as $(NH_4)_2SO_4$, NH_4HSO_4, KNO_3, K_2SO_4, or oxidized organic matter, implying that soot can provide important nuclei for the development of fine particles in the hazes.

Abundant KCl particles have been detected in fresh smoke plumes of biomass burning, and they are transformed through heterogeneous chemical reactions to K_2SO_4 and KNO_3 (Engling et al., 2009; Li et al., 2003; Pósfai et al., 2003; Adachi and Buseck, 2008). The dominance of K_2SO_4 and KNO_3 and absence of KCl in type-1 haze suggests that KCl from ABB presumably reacted with nitric acid and sulfuric acid in the atmosphere, prior to sampling. In addition,

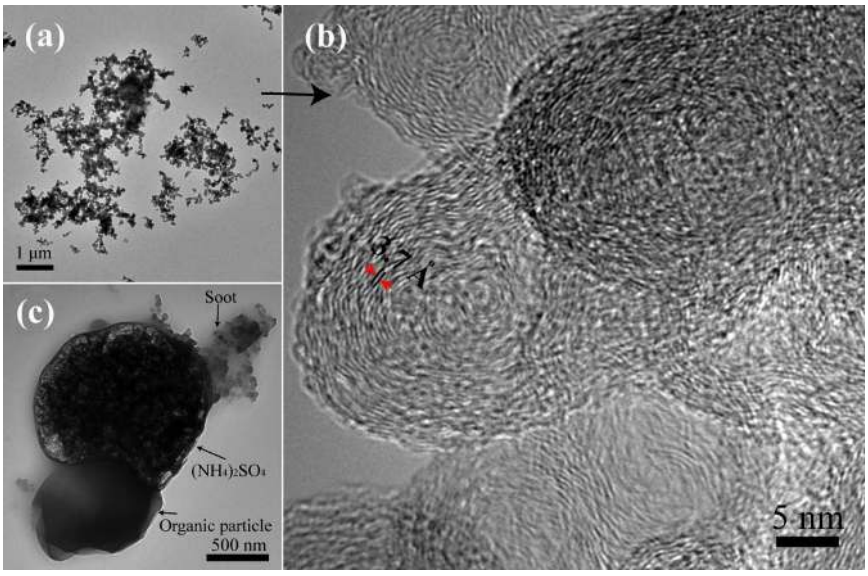

Fig. 6. TEM images of soot aggregates and organic matter. **(a)** TEM image of chain-like soot aggregate from the haze on 27 June. **(b)** High-magnification TEM image showing the onion-like structures and disordered graphitic layers typical of soot. **(c)** Mixture of organic matter, ammonium sulfate, and soot from the haze on 27 June.

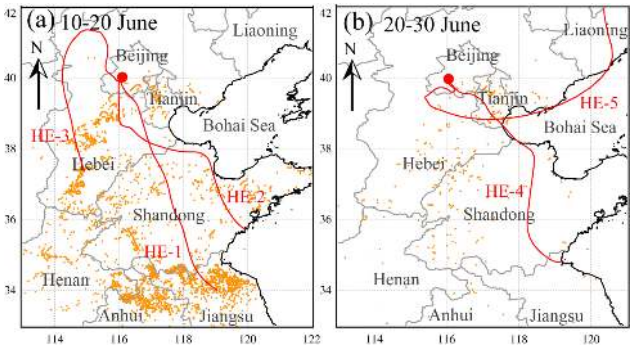

Fig. 7. Maps of northern China and five 48-h back trajectories (red lines) of air masses arriving at Beijing at a 500-m elevation (http://ready.arl.noaa.gov/HYSPLIT.php). **(a)** Areas of intense ABB during 10–20 June. The orange dots represent the positions of wildfires. **(b)** More disperse and fewer ABB spots during 21–30 June.

many S-rich particles in type-1 haze contain minor K (Fig. 5). A similar mixture was also observed in smoke hazes in Mexico (Yokelson et al., 2009).

4.2 Further considerations about regional brown hazes over China

Field observations show that all brown hazes display similarities such as low visibility and a high load of PM, but aerosol particles in different hazes exhibit different compositions, morphologies, and mixing states. Furthermore, differences in the chemical and physical properties of fine aerosol particles in different haze types (e.g., dust, brown smoke, and non-smoke brown haze) also impact the regional and global climates differently (Wang et al., 2009). Therefore, we need to identify haze types as well as the properties of individual aerosol particles in different hazes.

Emissions from ABB produce high concentrations of gases and fine particles for brief periods each year. These gases and particles enhance coagulation and condensation onto pre-existing aerosol particles, resulting in significant changes to their compositions, shapes, and mixing states (Bein et al., 2008). More importantly, however, high RH during brown hazes can promote the hygroscopic growth of K-rich, S-rich, and organic particles, or their mixtures. The positive correlation ($R = 0.9$) between AOD and WVC during the type-1 hazes (Fig. 9) suggests that large amounts of aerosol particles can grow hygroscopically (Li et al., 2007). Whenever the RH is elevated, its importance to the AOD is substantially amplified if the particles are hygroscopic (Bian et al., 2009). In addition, the AOD of aged soot in polluted air is increased over that of fresh soot and correlates strongly with RH (Zhang et al., 2008), leading to even greater decreases in visibility.

Morning and night relative humidity in June normally reaches 80% or higher but then decreases to between 20 and 60% from midday to late afternoon (Fig. S1). Therefore, when we consider the climate effects of aerosol particles in regional haze, the solid and aqueous states of the hygroscopic particles should be evaluated at different humidities. The variation of humidity during a haze episode can create cyclic changes of the soluble particles between the aqueous and solid states.

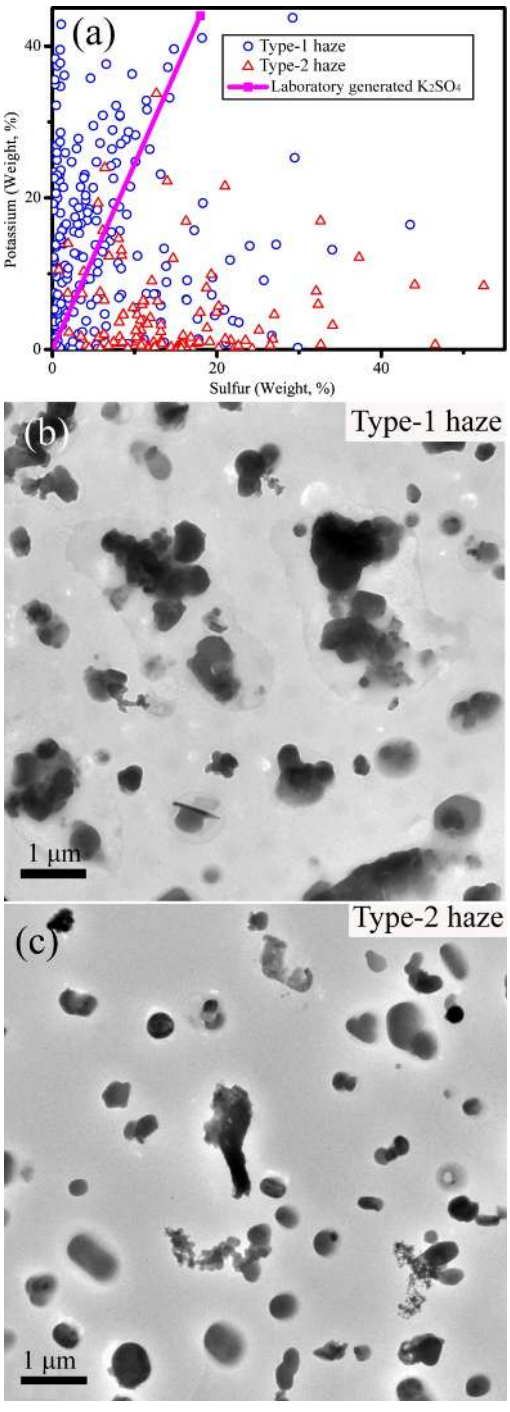

Fig. 8. Comparison of compositions and morphologies of individual fine particles from different haze episodes. **(a)** Separation of type-1 and -2 haze according to the S/K ratio of the respective aerosol particles. The open triangles represent the weight percentages of S and K in the measured particle. The solid line indicates the weight percentage of S and K from measurements of K_2SO_4 particles generated in the laboratory. All analyses were made using the same EDS instrument, yielding similar uncertainties, and are thus internally consistent. **(b)** Example of aerosol particles from a type-1 haze (17 June). **(c)** Example of aerosol particles from a type-2 haze (23 June).

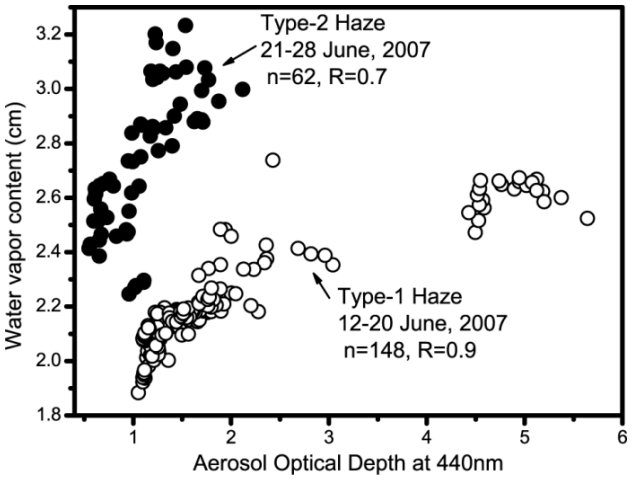

Fig. 9. Correlation between the AOD ("level 2.0, quality assured") at 440 nm and water vapor content during type-1 and -2 haze. Data points are from the NASA Aeronet network (http://aeronet.gsfc.nasa.gov/) and were obtained by sun photometers at 15-min intervals during the sampling period at the Beijing site, except that data points were excluded when it was cloudy or raining.

The high AOD values over northern China suggest that the haze particles reduce solar flux on the ground and cool the surface atmosphere. In contrast, the internally mixed soot particles in regional hazes absorb solar radiation and heat the upper atmosphere. Recent observations of radiative forcing from aerosols in regional hazes over northern China show that aerosol particles under hazy weather conditions generate a positive heating effect on the atmospheric column (Wang et al., 2009; Xia et al., 2006). Once aerosols alter the radiation budgets of the lower and upper atmospheres, a haze episode may persist because the atmosphere becomes more stable. Furthermore, the change may affect the development and microphysics of clouds by reducing vertical heat exchange and restricting convective transport (Fan et al., 2008). Significantly, these aged fine aerosol particles (Fig. 10) can be transported great distances and have the ability to carry toxic materials such as heavy metals and PAHs (Guilloteau et al., 2009; Li and Shao, 2009a). The adverse effects of these aerosol particles on human health merit serious attention.

5 Conclusions

The AOD from Giovanni map shows that the monthly average value of 550 nm in the region had its maximum (0.7) in June 2007. TEM/EDS measurements showed that potassium salts (K_2SO_4 and KNO_3) were abundant in fine particles collected during 12–20 June, and were minor during 21–30 June. To highlight the contrast, we grouped the haze episodes into two categories, with HE-1 to HE-3 (12–20 June) called "type-1 haze", and HE-4 to HE-5 (21–30 June)

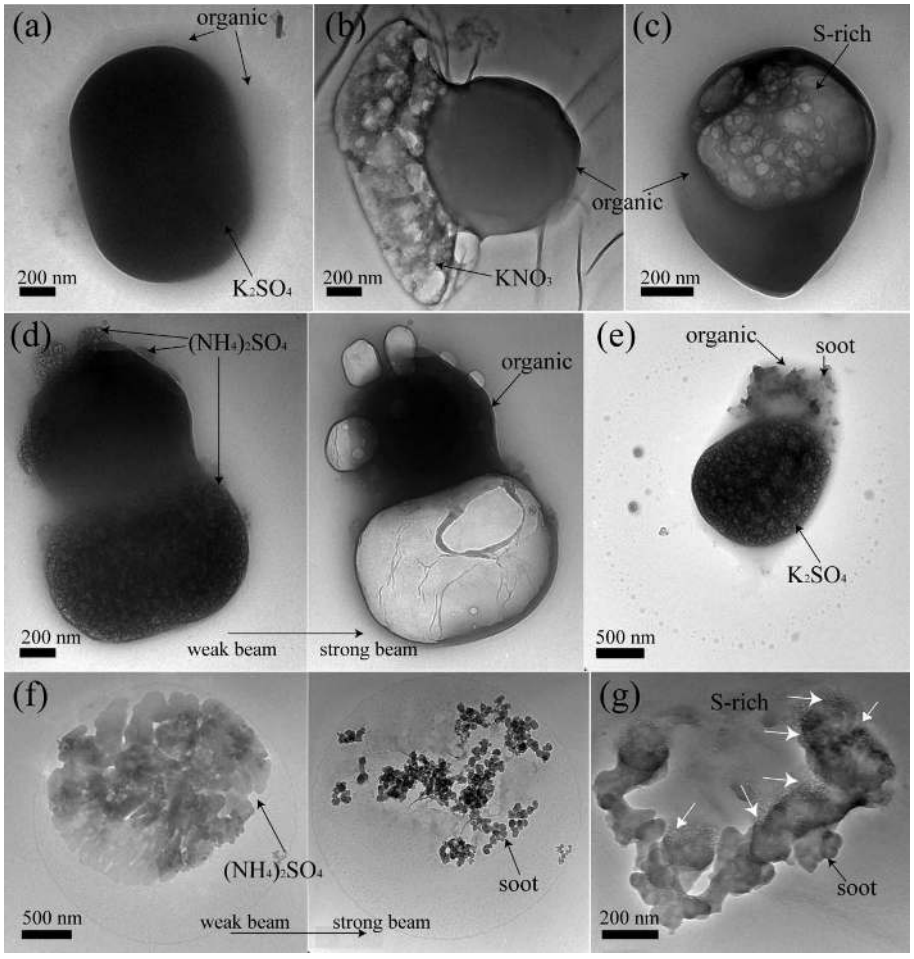

Fig. 10. Examples of mixtures of organic matter, K-rich and S-rich particles, and soot. **(a)** K_2SO_4 (beam damaged) with organic coating (12 June), **(b)** KNO_3 with organic matter (12 June), **(c)** S-rich particle with thick organic coating (19 June), **(d)** $(NH_4)_2SO_4$ with organic matter (19 June), **(e)** soot, organic matter, and K_2SO_4 (19 June), **(f)** soot embedded within $(NH_4)_2SO_4$ (20 June), **(g)** soot with S-rich coating (20 June).

called "type-2 haze." Consistent with MODIS wildfire maps and air mass back-trajectories, the abundant K-rich particles indicated that ABB contributed heavily to type-1 haze, and significantly influenced Beijing air quality.

The anthropogenic sources of aerosol particles contributing to the regular haze days (i.e., type-2 haze) in Beijing mainly consist of industry (steel and power plants), transportation, waste incineration, and cooking (Li and Shao, 2009a). However, the copious organic matter, soot particles, and gases emitted by ABB enhance the formation of secondary particles and the coagulation of pre-existing inorganic particles, resulting in more complex aerosol particles for type-1 haze than for type-2 haze.

Soot particles from ABB were generally mixed with potassium and ammonium salts, and organic matter. The aging of soot particles may increase the absorption of visible solar radiation when compared to soot alone (Jacobson, 2001; Adachi et al., 2010). In addition, abundant K_2SO_4 and KNO_3 in the absence of KCl illustrate that aerosol particles emitted by ABB reacted during their transport to the sampling site. Therefore, ABB emissions after atmospheric residence not only complicated the chemical transformation of aerosol particles during the transport but also changed their physical properties in downwind areas. Furthermore, the ABB contribution likely resulted in the doubling of the AOD due to type-1 haze relative to that of type-2 haze.

Supplementary material related to this article is available online at: http://www.atmos-chem-phys.net/10/8119/2010/acp-10-8119-2010-supplement.pdf.

Acknowledgements. We thank Wei Wang for assistance with sample collection and Evelyn Freney for providing two laboratory-generated samples of K_2SO_4 and KNO_3. We appreciate Kouji Adachi's comments, and acknowledge the use of the TEMs in

the LeRoy Eyring Center for Solid State Science at Arizona State University. Analyses and visualizations used in this study were produced with the Giovanni online data system, developed and maintained by the NASA Goddard Earth Sciences (GES) Data and Information Services Center (DISC). Financial support was provided by National Basic Research Program of China (2006CB403701), State Key Laboratory of Coal Resources and Safe Mining (SKLCRSM09KFB04), China Postdoctoral Science Foundation funded project (20090461213), and NSF grant ATM-0531926.

Edited by: D. Knopf

References

Acker, G. and Leptoukh, G.: Online Analysis Enhances Use of NASA Earth Science Data, Eos, Trans. AGU, 88(2), 14–17, 2007.

Adachi, K. and Buseck, P. R.: Internally mixed soot, sulfates, and organic matter in aerosol particles from Mexico City, Atmos. Chem. Phys., 8(21), 6469–6481, doi:10.5194/acp-8-6469-2008, 2008.

Adachi, K., Chung S. H., and Buseck P. R.: Shapes of soot aerosol particles and implications for their effects on climate, J. Geophys. Res., 115(D15), doi:10.1029/2009JD012868, 2010.

Andreae, M. O., Rosenfeld, D., Artaxo, P., Costa, A. A., Frank, G. P., Longo, K. M., and Silva-Dias, M. A. F.: Smoking Rain Clouds over the Amazon, Science, 303(5662), 1337–1342, 2004.

Bein, K. J., Zhao, Y. J., Johnston, M. V., and Wexler, A. S.: Interactions between boreal wildfire and urban emissions, J. Geophys. Res., 113(D07), D07304, doi:10.1029/2007JD008910, 2008.

Bian, H., Chin, M., Rodriguez, J. M., Yu, H., Penner, J. E., and Strahan, S.: Sensitivity of aerosol optical thickness and aerosol direct radiative effect to relative humidity, Atmos. Chem. Phys., 9(7), 2375–2386, doi:10.5194/acp-9-2375-2009, 2009.

Bowman, D. M. J. S., Balch, J. K., Artaxo, P., Bond, W. J., Carlson, J. M., Cochrane, M. A., D'Antonio, C. M., DeFries, R. S., Doyle, J. C., Harrison, S. P., Johnston, F. H., Keeley, J. E., Krawchuk, M. A., Kull, C. A., Marston, J. B., Moritz, M. A., Prentice, I. C., Roos, C. I., Scott, A. C., Swetnam, T. W., van der Werf, G. R., Pyne, S. J.: Fire in the Earth System, Science, 324(5926), 481–484, 2009.

Buseck, P. R. and Pósfai, M.: Airborne minerals and related aerosol particles: Effects on climate and the environment, P. Natl. Acad. Sci. USA, 96(7), 3372–3379, 1999.

Cao, G. L., Zhang, X. Y., Wang, Y. Q., and Zheng, F. C.: Estimation of emissions from field burning of crop straw in China, Chin. Sci. Bull., 53(5), 784–790, 2008.

Chung, S. H. and Seinfeld, J. H.: Global distribution and climate forcing of carbonaceous aerosols, J. Geophys. Res., 107 (D19), doi:10.1029/2001JD001397, 2002.

Crutzen, P. J. and Andreae, M. O.: Biomass burning in the tropics-impact on atmospheric chemistry and biogeochemical cycles, Science, 250(4988), 1669–1678, 1990.

Da Rocha, G. O., Allen, A. G., and Cardoso, A. A.: Influence of agricultural biomass burning on aerosol size distribution and dry deposition in southeastern Brazil, Environ. Sci. Technol., 39(14), 5293–5301, 2005.

de Gouw, J. A., Cooper, O. R., Warneke, C., Hudson, P. K., Fehsenfeld, F. C., Holloway, J. S., Hubler, G., Nicks, D. K., Nowak, J. B., Parrish, D. D., Ryerson, T. B., Atlas, E. L., Donnelly, S. G., Schauffler, S. M., Stroud, V., Johnson, K., Carmichael, G. R., Streets, D. G.: Chemical composition of air masses transported from Asia to the U. S. West Coast during ITCT 2K2: Fossil fuel combustion versus biomass-burning signatures, J. Geophys. Res.-Atmos., 109(D23), doi:10.1029/2003JD004202, 2004.

Du, W. P., Xin, J. Y., Wang, M. X., Gao, Q. X., Li, Z. Q., and Wang, Y. S.: Photometric measurements of spring aerosol optical properties in dust and non-dust periods in China, Atmos. Environ., 42(34), 7981–7987, 2008.

Duan, F. K., Liu, X. D., Yu, T., and Cachier, H.: Identification and estimate of biomass burning contribution to the urban aerosol organic carbon concentrations in Beijing, Atmos. Environ., 38(9), 1275–1282, 2004.

Eck, T. F., Holben, B. N., Reid, J. S., Dubovik, O., Smirnov, A., O'Neill, N. T., Slutsker, I., and Kinne, S.: Wavelength dependence of the optical depth of biomass burning, urban, and desert dust aerosols, J. Geophys. Res., 104(D24), 31333–31349, 1999.

Engling, G., Lee, J. J., Tsai, Y.-W., Lung, S.-C. C., Chou, C. C. K., Chan, and C.-Y.: Size-Resolved Anhydrosugar Composition in Smoke Aerosol from Controlled Field Burning of Rice Straw, Aerosol. Sci. Tech., 43(7), 662–672, 2009.

Fan, J., Zhang, R., Tao, W.-K., and Mohr, K. I.: Effects of aerosol optical properties on deep convective clouds and radiative forcing, J. Geophys. Res., 113(D08), doi:10.1029/2007JD009257, 2008.

Freney, E. J., Martin, S. T., and Buseck, P. R.: Deliquescence and Efflorescence of Potassium Salts Relevant to Biomass-Burning Aerosol Particles, Aerosol. Sci. Tech., 43(8), 799–807, 2009.

Fuller, K. A., Malm, W. C., and Kreidenweis, S. M.: Effects of mixing on extinction by carbonaceous particles, J. Geophys. Res., 104, 15941–15954, 1999.

Guilloteau, A., Bedjanian, Y., Nguyen, M. L., and Tomas, A.: Desorption of Polycyclic Aromatic Hydrocarbons from a Soot Surface: Three- to Five-Ring PAHs, J. Phys. Chem. A, 114(2), 942–948, 2009.

IPCC: Climate Change 2007: The Physical Science Basis, Contribution of Working Group I to the Fourth Assessment Report of the Intergovernmental Panel on Climate Change, edited by: Solomon, S., Qin, D., Manning, M., Chen, Z., Marquis, M., Averyt, K. B., Tignor, M., and Miller, H. L., Cambridge University Press, Cambridge, UK and New York, NY, USA, 2007.

Jacob, D. J., Crawford, J. H., Kleb, M. M., Connors, V. S., Bendura, R. J., Raper, J. L., Sachse, G. W., Gille, J. C., Emmons, L., and Heald, C. L.: Transport and Chemical Evolution over the Pacific (TRACE-P) aircraft mission: Design, execution, and first results, J. Geophys. Res., 108(D20), doi:10.1029/2002JD003276, 2003.

Jacobson, M. Z.: Strong radiative heating due to the mixing state of black carbon in atmospheric aerosols, Nature, 409(6821), 695–697, 2001.

Jaffe, D., Anderson, T., Covert, D., Kotchenruther, R., Trost, B., Danielson, J., Simpson, W., Berntsen, T., Karlsdottir, S., Blake, D., Harris, J., Carmichael, G., and Uno, I.: Transport of Asian air pollution to North America, Geophys. Res. Lett., 26(6), 711–714, 1999.

Jia, Y. T., Rahn, K. A., He, K. B., Wen, T. X., and Wang, Y. S.: A novel technique for quantifying the regional component of ur-

ban aerosol solely from its sawtooth cycles, J. Geophys. Res., 113(D21), doi:10.1029/2008JD010389, 2008.

Johnson, K. S., Zuberi, B., Molina, L. T., Molina, M. J., Iedema, M. J., Cowin, J. P., Gaspar, D. J., Wang, C., and Laskin, A.: Processing of soot in an urban environment: case study from the Mexico City Metropolitan Area, Atmos. Chem. Phys., 5, 3033-3043, doi:10.5194/acp-5-3033-2005, 2005.

Koe, L. C. C., Arellano, A. F., and McGregor, J. L.: Investigating the haze transport from 1997 biomass burning in Southeast Asia: its impact upon Singapore, Atmos. Environ., 35(15), 2723–2734, 2001.

Lesins, G., Chylek, P., and Lohmann, U.: A study of internal and external mixing scenarios and its effect on aerosol optical properties and direct radiative forcing, J. Geophys. Res., 107(D10), doi:10.1029/2001JD000973, 2002.

Li, J., Pósfai, M., Hobbs, P. V., and Buseck, P. R.: Individual aerosol particles from biomass burning in southern Africa: 2, Compositions and aging of inorganic particles, J. Geophys. Res., 108(D13), doi:10.1029/2002JD002310, 2003.

Li, L. J., Wang, Y., Zhang, Q., Li, J. X., Yang, X. G., and Jin, J.: Wheat straw burning and its associated impacts on Beijing air quality, Sci. China Ser. D-Earth Sci., 51(3), 403–414, 2008.

Li, W. J. and Shao, L. Y.: Transmission electron microscopy study of aerosol particles from the brown hazes in northern China, J. Geophys. Res., 114(D09), doi:10.1029/2008JD011285, 2009a.

Li, W. J. and Shao, L. Y.: Observation of nitrate coatings on atmospheric mineral dust particles, Atmos. Chem. Phys., 9(6), 1863–1871, doi:10.5194/acp-9-1863-2009, 2009b.

Li, W. J. and Shao, L. Y.: Mixing and water-soluble characteristics of particulate organic compounds in individual urban aerosol particles, J. Geophys. Res., 115(D02), doi:10.1029/2009JD012575, 2010.

Li, Z. Q., Xia, X. G., Cribb, M., Mi, W., Holben, B., Wang, P. C., Chen, H. B., Tsay, S. C., Eck, T. F., Zhao, F. S., Dutton, E. G., and Dickerson, R. E.: Aerosol optical properties and their radiative effects in northern China, J. Geophys. Res., 112(D22), doi:10.1029/2006JD007382, 2007.

Ma, Y., Weber, R. J., Lee, Y. N., Orsini, D. A., Maxwell-Meier, K., Thornton, D. C., Bandy, A. R., Clarke, A. D., Blake, D. R., Sachse, G. W., Fuelberg, H. E., Kiley, C. M., Woo, J. H., Streets, D. G., and Carmichael, G. R.: Characteristics and influence of biosmoke on the fine-particle ionic composition measured in Asian outflow during the Transport and Chemical Evolution Over the Pacific (TRACE-P) experiment, J. Geophys. Res., 108(D21), doi:10.1029/2002JD003128, 2003.

Niemi, J. V., Tervahattu, H., Vehkamaki, H., Martikainen, J., Laakso, L., Kulmala, M., Aarnio, P., Koskentalo, T., Sillanpaa, M., and Makkonen, U.: Characterization of aerosol particle episodes in Finland caused by wildfires in Eastern Europe, Atmos. Chem. Phys., 5, 2299–2310, doi:10.5194/acp-5-2299-2005, 2005.

Peltier, R. E., Hecobian, A. H., Weber, R. J., Stohl, A., Atlas, E. L., Riemer, D. D., Blake, D. R., Apel, E., Campos, T., and Karl, T.: Investigating the sources and atmospheric processing of fine particles from Asia and the Northwestern United States measured during INTEX B, Atmos. Chem. Phys., 8(6), 1835–1853, doi:10.5194/acp-8-1835-2008, 2008.

Pósfai, M., Anderson, J. R., Buseck, P. R., and Sievering, H.: Soot and sulfate aerosol particles in the remote marine troposphere, J. Geophys. Res., 104(D17), 21685–21693, 1999.

Pósfai, M., Simonics, R., Li, J., Hobbs, P. V., and Buseck, P. R.: Individual aerosol particles from biomass burning in southern Africa: 1. Compositions and size distributions of carbonaceous particles, J. Geophys. Res., 108(D13), doi:10.1029/2002JD002291, 2003.

Pósfai, M. and Buseck, P. R.: Nature and climate effects of individual tropospheric aerosol particles, Ann. Rev. Earth Planet. Sci., 38(1), 17–43, 2010.

Ramanathan, V. and Carmichael, G.: Global and regional climate changes due to black carbon, Nature Geosci, 1(4), 221–227, 2008.

Reid, J. S., Hobbs, P. V., Ferek, R. J., Blake, D. R., Martins, J. V., Dunlap, M. R., and Liousse, C.: Physical, chemical, and optical properties of regional hazes dominated by smoke in Brazil, J. Geophys. Res., 103(D24), 32059–32080, 1998.

Reid, J. S., Koppmann, R., Eck, T. F., and Eleuterio, D. P.: A review of biomass burning emissions part II: intensive physical properties of biomass burning particles, Atmos. Chem. Phys., 5, 799–825, doi:10.5194/acp-5-799-2005, 2005.

Roberts, G. C., Nenes, A., Seinfeld, J. H., and Andreae, M. O.: Impact of biomass burning on cloud properties in the Amazon Basin, J. Geophys. Res., 108(D2), doi:10.1029/2001JD000985, 2003.

Shao, L. Y., Li, W. J., Xiao, Z. H., and Sun, Z. Q.: The mineralogy and possible sources of spring dust particles over Beijing, Adv. Atmos. Sci., 25(3), 395–403, 2008.

Sheridan, P. J., Schnell, R. C., Kahl, J. D., Boatman, J. F., and Garvey, D. M.: Microanalysis of the aerosol collected over south-central New Mexico during the alive field experiment, May–December 1989, Atmos. Environ., 27(8), 1169–1183, 1993.

Wang, Y., Che, H., Ma, J., Wang, Q., Shi, G., Chen, H., Goloub, P., and Hao, X.: Aerosol radiative forcing under clear, hazy, foggy, and dusty weather conditions over Beijing, China, Geophys. Res. Lett., 36, L06804, doi:10.1029/2009GL037181, 2009.

Xia, X. A., Chen, H. B., Wang, P. C., Zhang, W. X., Goloub, P., Chatenet, B., Eck, T. F., and Holben, B. N.: Variation of column-integrated aerosol properties in a Chinese urban region, J. Geophys. Res., 111, D05204, doi:10.1029/2005JD006203, 2006.

Yang, M., Howell, S. G., Zhuang, J., and Huebert, B. J.: Attribution of aerosol light absorption to black carbon, brown carbon, and dust in China – interpretations of atmospheric measurements during EAST-AIRE, Atmos. Chem. Phys., 9(6), 2035–2050, doi:10.5194/acp-9-2035-2008, 2009.

Yao, X., Lau, A. P. S., Fang, M., Chan, C. K., and Hu, M.: Size distributions and formation of ionic species in atmospheric particulate pollutants in Beijing, China: 1-inorganic ions, Atmos. Environ., 37(21), 2991–3000, 2003.

Yienger, J. J., Galanter, M., Holloway, T. A., Phadnis, M. J., Guttikunda, S. K., Carmichael, G. R., Moxim, W. J., and Levy, H.: The episodic nature of air pollution transport from Asia to North America, J. Geophys. Res.-Atmos., 105(D22), 26931–26945, 2000.

Yokelson, R. J., Crounse, J. D., DeCarlo, P. F., Karl, T., Urbanski, S., Atlas, E., Campos, T., Shinozuka, Y., Kapustin, V., Clarke, A. D., Weinheimer, A., Knapp, D. J., Montzka, D. D., Holloway, J., Weibring, P., Flocke, F., Zheng, W., Toohey, D., Wennberg, P. O., Wiedinmyer, C., Mauldin, L., Fried, A., Richter, D., Walega, J., Jimenez, J. L., Adachi, K., Buseck, P. R., Hall, S. R., and Shet-

ter, R.: Emissions from biomass burning in the Yucatan, Atmos. Chem. Phys., 9(15), 5785–5812, doi:10.5194/acp-9-5785-2009, 2009.

Zhang, R. Y., Khalizov, A. F., Pagels, J., Zhang, D., Xue, H. X., and McMurry, P. H.: Variability in morphology, hygroscopicity, and optical properties of soot aerosols during atmospheric processing, P. Natl. Acad. Sci. USA, 105(30), 10291–10296, 2008.

Zhang, X. Y., Gong, S. L., Shen, Z. X., Mei, F. M., Xi, X. X., Liu, L. C., Zhou, Z. J., Wang, D., Wang, Y. Q., and Cheng, Y.: Characterization of soil dust aerosol in China and its transport and distribution during 2001 ACE-Asia: 1. Network observations, J. Geophys. Res.,, 108(D9), doi:10.1029/2002JD002632, 2003.

Zhang, Y. X., Shao, M., Zhang, Y. H., Zeng, L. M., He, L. Y., Zhu, B., Wei, Y. J., Zhu, and X. L.: Source profiles of particulate organic matters emitted from cereal straw burnings, J. Environ. Sci., 19(2), 167–175, 2007.